Chapter 4
Field Evolution Within the Framework of the Burgers Equation

In this chapter, we describe some solutions of the Burgers equation for single-scale fields, discuss properties of solutions to the Burgers equation for multi-scale fields, which, in one way or another, help to understand laws of evolution of noise fields.

4.1 Evolution of one-dimensional signals

Let us discuss typical scenarios of evolution of solutions to the Burgers equation realized under various initial conditions. We pay special attention to strongly nonlinear regimes, and also to specific features of the way a solution of the Burgers equation approaches the linear stage.

Solutions of the Burgers equation, typical for nonlinear acoustics, are also discussed in Refs. [1, 2] and in the second part of the present book.

4.1.1 Self-similar solution, once more

Let us return to the solution (3.84) of the Burgers equation. It is easy rigorously to prove that it exists at any $t \in (0,\infty)$ and gives the unique solution of the Cauchy problem (3.77), if $v_0(x)$ grows at $x \to \pm\infty$ slower than the first power of x:

$$|v_0(x)| < A + B|x|^{\gamma} \quad (x \in \mathbb{R},\ A,B < \infty,\ 0 \leqslant \gamma < 1). \tag{4.1}$$

Note, however, that while this condition of existence and uniqueness guarantees availability of a solution to the Burgers equation, it does not prohibit to seek other solutions of this equation with initial conditions, which are beyond the framework of the inequalities (4.1). Sometimes such "exotic" solutions are very instructive for theory and valuable for applications. The Khokhlov solution (3.34), its particular case (3.39) or even the simplest solution of this class (3.18) satisfying a linear initial

S. N. Gurbatov et al., *Waves and Structures in Nonlinear Nondispersive Media*
© Higher Education Press, Beijing and Springer-Verlag Berlin Heidelberg 2011

condition $v_0(x) = \alpha x$ serve as examples. Its exoticism consists in that at $\alpha < 0$ the field (3.18) "lives" only for a finite time, everywhere turning to infinity at $t^* = 1/|\alpha|$. But even this trivial "end of the world" may serve as a convenient model of the gradient catastrophe known from the previous chapter.

Example. Let us find a solution of the Burgers equation with the initial condition

$$v_0(x) = S\delta(x). \tag{4.2}$$

We already know the corresponding field $v(x,t)$, because we earlier established that the self-similar solution (3.49) weakly converges at $t \to 0$ to the delta function. Nevertheless, it is always useful to investigate different paths towards one and the same solution, since, as a rule, this helps shed new light upon the problem at hand.

The initial potential $s_0(x) = S\Theta(x)$ corresponds to the initial condition (4.2). Consequently, the initial condition for the auxiliary linear diffusion equation (3.78) is representable in the following form:

$$\varphi_0(x) = 1 - (1 - e^{-\mathrm{R}})\Theta(x).$$

By substituting it into the solution (3.80) of the diffusion equation, we have

$$\varphi(x,t) = 1 - (1 - e^{-\mathrm{R}})\Phi\left(\frac{x}{2\sqrt{\mu t}}\right). \tag{4.3}$$

Here R is the initial Reynolds number familiar from the self-similar solution, and $\Phi(z)$ is the auxiliary function (3.44).

By substituting (4.3) into (3.76), we find the sought-for solution of the Burgers equation with a singular initial condition. Naturally, it coincides with the self-similar solution (3.49). But this does not mean that we have wasted our time by looking for an already known solution. Based on the experience of solving the linear diffusion equation, we will formulate a statement radically changing our understanding of the role of the self-similar solution. Until now we have thought it to be one of particular solutions of the Burgers equation. Now we are capable, based on the obtained general solution and the theory of the linear diffusion equation, of rigorously proving that:
if the integral of the initial condition $v_0(x)$ is finite and equal to

$$\int_{-\infty}^{\infty} v_0(x)\,dx = S,$$

then at $t \to \infty$ the solution $v(x,t)$ of the Burgers equation asymptotically tends to the self-similar solution (3.49) with the Reynolds number $\mathrm{R} = S/2\mu$.

Thus, self-similar solutions serve as a powerful instrument for analysis of asymptotic properties of solutions to nonlinear equations. ∎

Note. We note that the above statement contradicts "common sense", according to which the current Reynolds number, due to dissipation of an acoustic wave in a viscous ($\mu \neq 0$) medium, must tend to zero ($\mathrm{R} \to 0$, $t \to \infty$), and the field, sooner or

later, enters the linear stage of its evolution. We see that in the case under discussion, this is not so: The characteristic amplitude of the field $U(t)$ (3.60) indeed tends to zero at $t \to \infty$, but, at the same time, at the same rate grows the external length-scale $\ell(t)$ (3.59). As a result, the Reynolds number remains constant, and nonlinearity, as before, substantially determines the form of the field's profile.

4.1.2 Approach to the linear stage

Note that the above mentioned "common sense" does not let us down, is the initial field has a wave-like character:

$$\int_{-\infty}^{\infty} v_0(x)\,dx = 0. \tag{4.4}$$

In this case, at any, however large initial Reynolds number R, the solution of the Burgers equation eventually is asymptotically described by the linear diffusion equation. In other words, the nonlinear stage of evolution of the field $v(x,t)$ is succeeded by the linear stage.

Let us find the asymptotic of the solution of the Burgers equations at the linear stage. Note that the equality (4.4), as applied to the potential $s_0(x)$ of the initial field $v_0(x)$, means that the limiting values of $s_0(x)$ at $x \to \pm\infty$ are the same:

$$\lim_{x\to-\infty} s_0(x) = \lim_{x\to\infty} s_0(x).$$

Since the potential is defined with an accuracy up to an arbitrary constant, we assign these limits to be equal to zero. In other words, the initial potential is *localized* in a certain region of the x-axis. In order for the further constructions to be more rigorous, we require, for definitiveness, the initial potential $s_0(x)$ to be a finite functions, not equal to zero only within the interval $|x| < \ell$. Then the initial condition for the corresponding linear diffusion equation (3.78) assume the following form:

$$\varphi_0(x) = 1 + q_0(x), \tag{4.5}$$

where

$$q_0(x) = \exp\left(-\frac{s_0(x)}{2\mu}\right) - 1 \tag{4.6}$$

is also a finite function identically equal to zero at $|x| \geqslant \ell$.

From the properties of linear diffusion equations, it is known that if

$$t \gg t_d, \quad t_d = \frac{\ell^2}{4\mu}, \tag{4.7}$$

then the solution of Eq. (3.78) with the initial condition (4.5) is described by the asymptotic formula

$$\varphi(x,t) \sim 1 + Q(t) \exp\left(-\frac{x^2}{4\mu t}\right). \tag{4.8}$$

Here

$$Q(t) = \frac{Q_0}{2\sqrt{\pi\mu t}}, \quad Q_0 = \int_{-\infty}^{\infty} q_0(y)\, dy. \tag{4.9}$$

By substituting the asymptotic formula (4.8) into the right-hand side of the relationship (3.76), we obtain the asymptotic of the solution to the Burgers equation

$$v(x,t) \sim \frac{x}{t} \frac{Q(t)}{\exp\left(\frac{x^2}{4\mu t}\right) + Q(t)}. \tag{4.10}$$

The function $Q(t)$, which enters this expression, with time monotonically tends to zero. Hence, at $t \gg t_l$, where t_l is the characteristic time of approach to the linear regime:

$$Q(t_l) \simeq 1 \Rightarrow t_l = \frac{Q_0^2}{4\pi\mu}, \tag{4.11}$$

the asymptotic of the solution to the Burgers equation (3.77) will practically coincide with the solution of the linear diffusion equation

$$v(x,t) \sim \frac{x}{t} \frac{Q_0}{2\sqrt{\pi\mu t}} \exp\left(-\frac{x^2}{4\mu t}\right). \tag{4.12}$$

4.1.3 N-wave and U-wave

Earlier, we have found the characteristic time t_l (4.11) of approach of the solution to the Burgers equation to the linear regime. But this time itself, and also the mechanism of the transition to the linear stage, strongly depend on the shape of the initial field $v_0(x)$. In the nonlinear wave theory, there are even special terms: *N-wave* and *U-wave* [1], in order to distinguish regimes of evolution of nonlinear waves and their transition to the linear stage. Below we consider examples illustrating the notion of N- and U-waves.

Example 1. Let the initial field equal the difference of the two delta functions

$$v_0(x) = S[\delta(x+\ell) - \delta(x-\ell)]. \tag{4.13}$$

To this field correspond the rectangular potential $s_0(x)$ and function $q_0(x)$ (4.6):

[1] Note that in nonlinear acoustics, where the graphs of an acoustic field can be found by a mirror reflection of the studied in this section solutions of the Burgers equation, different terminology is used. So N-waves, discussed here, correspond to acoustic S-waves, and U-waves correspond to acoustic N-waves.

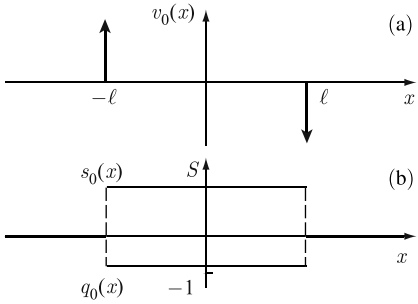

Fig. 4.1 Initial field $v_0(x)$ (4.13) **(a)** and fields $s_0(x)$, $q_0(x)$ **(b)**.

$$s_0(x) = [\Theta(x+\ell) - \Theta(x-\ell)],$$
$$q_0(x) = \left(e^{-\mathrm{R}} - 1\right)[\Theta(x+\ell) - \Theta(x-\ell)]. \tag{4.14}$$

The initial condition (4.13) and functions (4.14) are plotted in Fig. 4.1.

In (4.14), the initial Reynolds number (3.47) $R = S/2\mu$ is introduced. In the most interesting case $R \gg 1$ from (4.14), (4.9), (4.11) we have

$$q_0(x) \simeq -[\Theta(x+\ell) - \Theta(x-\ell)] \Rightarrow Q_0 \simeq -2\ell \Rightarrow t_l \simeq \frac{4}{\pi} t_d.$$

Thus, in this case, the time of approach to the linear stage is close to the characteristic time of linear diffusion t_d (4.7).

Let us trace stages of evolution of the field $v(x,t)$ corresponding to the initial condition (4.13), by using the exact solution of the Burgers equation:

$$v(x,t) = -\frac{2\mu}{\ell}\sqrt{\frac{\mathrm{R}}{\pi\tau}}\frac{\left(1-e^{-\mathrm{R}}\right)\exp\left(-\mathrm{R}\frac{z^2+1}{\tau}\right)\sinh\left(\frac{2\mathrm{R}z}{\tau}\right)}{1-(1-e^{-\mathrm{R}})\left[\Phi\left(\sqrt{\frac{\mathrm{R}}{\tau}}(1-z)\right) - \Phi\left(-\sqrt{\frac{\mathrm{R}}{\tau}}(1+z)\right)\right]}. \tag{4.15}$$

Here we introduced the dimensionless coordinate and time $z = x/\ell$, $\tau = 2St/\ell^2$, and the function Φ is defined by the equality (3.44). The field $v(x,t)$ is plotted in Fig. 4.2 for different values of τ and at $\mathrm{R} = 25$ At the moment of time $\tau = 0.5$, the field consists of two triangular waves. At $\tau = 1$, the triangular waves collided and started to "devour" each other. At $\tau = 2$, mutual absorption of the triangular waves strongly decreases their amplitude. But the absolute magnitude of the parameter (4.9)

$$Q(\tau) \simeq -\sqrt{\frac{4\mathrm{R}}{\pi\tau}}$$

is still appreciable ($|Q(\tau = 1)| \simeq 4$), and the nonlinear stage of evolution still continues. Characteristic features of the field $v(x,t)$ at $\tau = 1$ and $\tau = 2$, having the shape of a stylized letter N, are reflected in the way such type nonlinear fields are referred to: N-waves. Finally, at $\tau = \mathrm{R} = 30$, when $|Q(\tau = 30)| \simeq 1$, mutual annihilation of the triangular waves ends in entering the linear stage. ∎

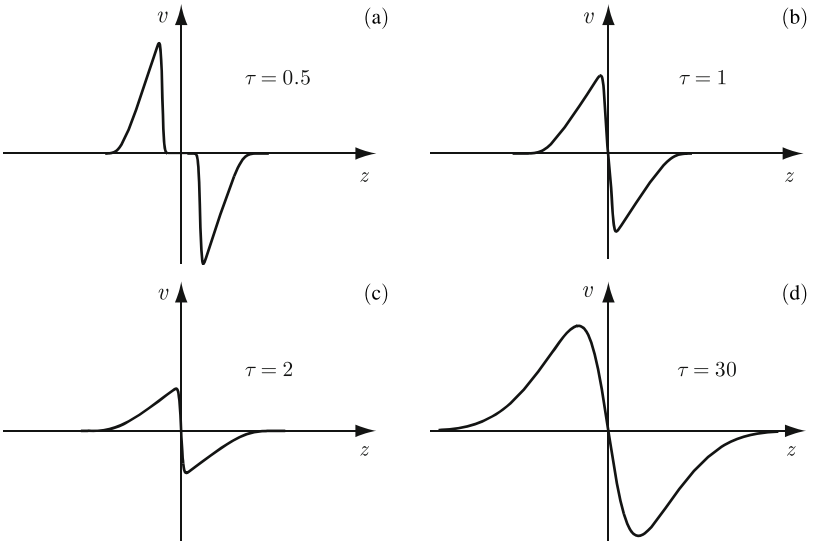

Fig. 4.2 Solution of the Burgers equation of the N-wave type, with the initial condition (4.13) and initial Reynolds number R=25, at different moments of time. The scales of the horizontal axes match, and the vertical scale of the latter graph is much greater than the scale of the former ones, in order for the weakened by dissipation solution of the Burgers equation at the linear stage to be seen.

Example 2. We obtain an example of U-waves by studying the solution of the Burgers equation with the initial condition

$$v_0(x) = S[\delta(x-\ell) - \delta(x+\ell)]. \tag{4.16}$$

The corresponding exact solution

$$v(x,t) = -\frac{2\mu}{\ell}\sqrt{\frac{\mathrm{R}}{\pi\tau}}\,\frac{\left(1-e^{\,\mathrm{R}}\right)\exp\left(-\mathrm{R}\frac{z^2+1}{\tau}\right)\sinh\left(\frac{2\mathrm{R}z}{\tau}\right)}{1-(1-e^{\mathrm{R}})\left[\Phi\left(\sqrt{\frac{\mathrm{R}}{\tau}}(1-z)\right)-\Phi\left(-\sqrt{\frac{\mathrm{R}}{\tau}}(1+z)\right)\right]}, \tag{4.17}$$

is, at the first sight, very similar to the solution (4.15). But its behavior drastically differs from the behavior of the N-wave considered above in that the triangular waves, generated by the delta-like components of the initial condition (4.16), travel away from each other (see. Fig. 4.3). Therefore, in contrast to the N-wave, the triangular components of the U-wave interact only with their "tails". At a large R, this interaction is much weaker than the mutual extinguishing of the fronts for N-waves. As a result, the nonlinear stage of U-waves lasts much longer than for N-waves.

Let us confirm the above-said by quantitate derivations, by computing the time (4.11) of approach to the linear stage. In this case, it is equal to

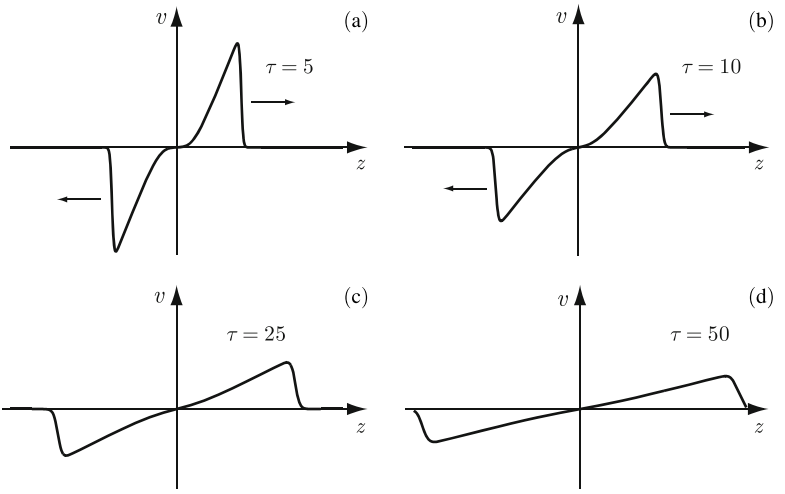

Fig. 4.3 Solution of the Burgers equation of the U-wave type with the initial condition (4.16) and R=25, at different moments of time.

$$t_l = \frac{4}{\pi}\left(e^{\mathrm{R}} - 1\right) t_d.$$

Hence, at the same (large) initial Reynolds number, the nonlinear stage of a U-wave lasts unimaginably longer than that of an N-wave. So, for the initial Reynolds number used in the examples $\mathrm{R} = 25$, the time of approach to the linear stage for the U-wave is approximately 10^{10} times greater than that for the N-wave. ∎

Note. Let us emphasize the importance of the notion of N- and U-waves. They describe typical elements of universal nonlinear structures appearing in the process of evolution of nonlinear fields with various initial conditions. Universality of N- and U-waves is expressed by the fact that the asymptotic formula (4.10) does not depend on fine details of the initial conditions $v_0(x)$, but does depend only on their integral characteristic Q_0 (4.9). If the latter quantity is positive, the field with acquires an N-like shape, whereas if $Q_0 < 0$, the field "rolls down" to a U-wave.

4.1.4 Sawtooth waves

Until now we used to specify an initial field $v_0(x)$ and monitor the corresponding solution of the Burgers equation. Sometimes, another approach is no less fruitful, whereby an initial condition $\varphi_0(x)$ of the linear diffusion equation (4.11) is given and the generated by it solution of the Burgers equation is studied. In what follows, the above mentioned approach will allow us illustratively to clarify the notion of *sawtooth waves* playing a key role in the analysis of behavior of nonlinear fields satisfying the Burgers equation.

Example. Let us take an initial condition of the linear diffusion equation (3.78) as the sum of delta functions:

$$\varphi_0(x) = \delta(x+\ell) + Q^2\delta(x-\ell). \tag{4.18}$$

Up to a common factor, which does not depend on x. the solution of the linear diffusion equation (3.78) has the following form:

$$\varphi(x,t) = \exp\left(-\frac{(x+\ell)^2}{4\mu t}\right) + Q^2\exp\left(-\frac{(x-\ell)^2}{4\mu t}\right).$$

By substituting it into (3.76) and reducing the common factor factors in the numerator and denominator, we have

$$v(x,t) = \frac{x}{t} - \frac{\ell}{t}\,\frac{Q^2\exp\left(\frac{x\ell}{2\mu t}\right) - \exp\left(-\frac{x\ell}{2\mu t}\right)}{Q^2\exp\left(\frac{x\ell}{2\mu t}\right) + \exp\left(-\frac{x\ell}{2\mu t}\right)}.$$

We will better understand the physical meaning of the parameter Q by representing it in the following form:

$$Q = \exp\left(-\frac{s}{2\mu}\right). \tag{4.19}$$

As a result, we finally obtain

$$v(x,t) = \frac{1}{t}\left[x - \ell\tanh\left(\frac{\ell}{2\mu t}(x-Vt)\right)\right], \quad V = \frac{s}{\ell}.$$

This is the already familiar (but moving at a velocity V) solution (3.39) of the Burgers equation. By giving the artificial initial condition (4.18), we arrived at a natural, having a visual physical meaning solution of the Burgers solution. ∎

Let us build on the success by taking $\varphi_0(x)$ in the form of an arbitrary superposition of delta functions:

$$\varphi_0(x) = \sum_k Q_k\,\delta(x-y_k), \tag{4.20}$$

and in analogy with (4.19), assigning the coefficients to be equal to

$$Q_k = \exp\left(-\frac{s_k}{2\mu}\right). \tag{4.21}$$

Let us call the field corresponding to the initial condition (4.20) a *sawtooth wave*. Let us write the sawtooth wave in the form (3.84)

$$v(x,t) = \frac{x - \{y\}(x,t)}{t}, \tag{4.22}$$

where $\{y\}(x,t)$ is the mean Lagrangian coordinate, which here is equal to

$$\{y\}(x,t) = \frac{\sum\limits_k y_k \exp\left(-\frac{1}{2\mu t}\left[s_k t + \frac{(x-y_k)^2}{2}\right]\right)}{\sum\limits_k \exp\left(-\frac{1}{2\mu t}\left[s_k t + \frac{(x-y_k)^2}{2}\right]\right)}. \tag{4.23}$$

In order more clearly to comprehend the geometric meaning of the obtained solution, let us pick out the skeleton of the mean Lagrangian coordinate $\{y\}(x,t)$ and the corresponding skeleton of the sawtooth wave $v(x,t)$. Obviously, at $\mu \to 0_+$, in each point x, is sufficient to retain one (the largest) term in both numerator and denominator of Eq. (4.23). The dominant term is determined by plotting graphs of the *critical parabolas*

$$\Pi_k(x) = s_k t + \frac{(x-y_k)^2}{2}, \tag{4.24}$$

and choosing that one, which, in the point x, is less than the rest of them. Accordingly, $\{y\}(x,t)$ turns out to be a stepwise function, which is equal to

$$\{y\}(x,t) = y_k,$$

where k is the number of a given parabola. At the points of intersection of the lowest critical parabolas, the skeleton of the function $\{y\}(x,t)$ has discontinuities. Let us find the points $x_{k,m}(t)$ if intersection of the kth and mth parabolas:

$$\begin{gathered} \Pi_k(x) = \Pi_m(x) \Rightarrow x_{k,m}(t) = x^0_{k,m} + V_{k,m}\, t, \\ x^0_{k,m} = \frac{y_k + y_m}{2},\ V_{k,m} = \frac{s_m - s_k}{M_{km}},\ M_{k,m} = y_m - y_k \quad (k < m). \end{gathered} \tag{4.25}$$

If, immediately to the left and right of the point $x_{k,m}(t)$, the parabolas Π_k and Π_m are less than the other parabolas, then at the point $x_{k,m}(t)$ the function $\{y\}(x,t)$ undergoes a discontinuity. Thereby

$$\{y\}(x_{k,m}(t) - 0, t) = y_k, \quad \{y\}(x_{k,m}(t) + 0, t) = y_m \quad (k < m).$$

Critical parabolas (4.24) illustrating the construction of a stepwise function $\{y\}(x,t)$ are shown in Fig. 4.4.

If the discontinuities (shocks) move at different velocities $V_{k,m}$, some of them coalesce forming a new shock moving at its own velocity. Let us study the laws of coalescence of shocks in detail.

Let in a small neighborhood of $t \in (t_{k,m,n} - \varepsilon, t_{k,m,n})$ of the moment $t_{k,m,n}$ of intersection of the straight lines $x_{k,m}(t)$ and $x_{m,n}(t)$, and in a small neighborhood of the intersection point $x_{k,m,n}$, the smallest parabolas consecutively are Π_k, Π_m and Π_n $(k < m < n)$. This means that at the points $x_{k,m}(t)$ and $x_{m,n}(t)$ the function $\{y\}(x,t)$ has discontinuities. At the moment of time $t_{k,m,n}$, the middle parabola Π_m happens to be everywhere higher than the other ones, and at the position of two coalesced shocks, a new one emerges, with the coordinate $x_{k,n}(t)$ and velocity $V_{k,n}$. From (4.25) follows that the velocity of the shock created at the point of coalescence of the old shocks is connected with the velocities of the latter ones by the following equality:

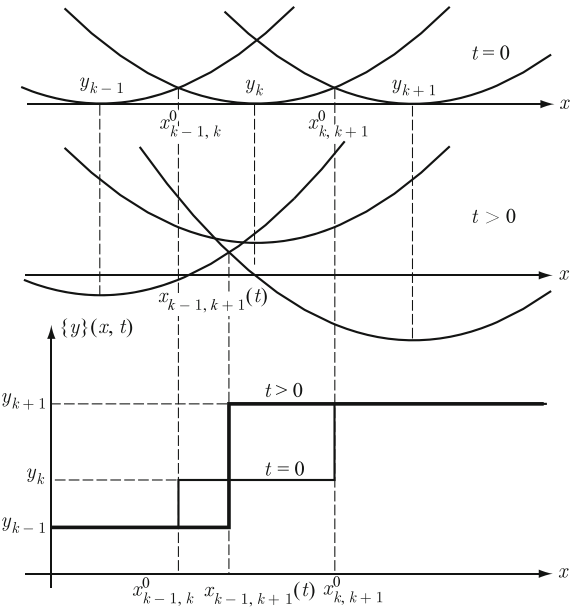

Fig. 4.4 Illustration to the construction of the skeleton of the function $\{y\}(x,t)$ by means of the comparison of parabolas. At the top, the parabolas at $t=0$, and below, the parabolas at $t>0$ are shown. It is seen that the middle parabola is everywhere higher than at least one of the rest parabolas. Therefore, instead of two discontinuities of the function $\{y\}(x,t)$ at the points $x^0_{k-1,k}$ and $x^0_{k,k+1}$, only one discontinuity is left at the point $x_{k-1,k+1}(t)$.

$$V_{k,n}=\frac{s_n-s_k}{y_n-y_k}=\frac{M_{k,m}V_{k,m}+M_{m,n}V_{m,n}}{M_{k,m}+M_{m,n}}. \tag{4.26}$$

This formula coincides with the law of velocity change of particles with masses $M_{k,m}$ and $M_{m,n}$ at an absolutely inelastic collision.

The fact that, until coalescence, the shock velocities are constant, and at the moment of coalescence they change according to the law of absolutely inelastic collisions, allows us to describe the behavior of a sawtooth wave in the parlance of a one-dimensional flow of inelastically colliding particles. The constructed according to the formula (3.84) skeleton of the sawtooth field $v(x,t)$ is shown in Fig. 4.5. The typical pattern of the trajectories of coalescing shocks is depicted in Fig. 4.6.

Until now we studied the skeleton of a sawtooth wave corresponding to the limit $\mu\to 0_+$. The expression (4.23) for the mean coordinate $\{y\}(x,t)$, however, also describes the smearing of the shocks because of viscosity ($\mu>0$) and the approach to the linear stage. The latter is reached, when for any x the neighboring terms in the sums (4.23) have comparable magnitudes.

Let us briefly discuss an application scheme of the sawtooth-wave approximation. In order to do this, we recall the initial condition of the linear diffusion equation (4.6). Let s_k be the minimum value of the initial potential $s_0(x)$ attained at the point $x=y_k$. Then, at small μ and in a vicinity of the position of the minimum, this function may be replaced by the Gaussian:

$$\varphi_0^k(x)\sim\exp\left[-\frac{s_k}{2\mu}-\frac{\sigma_k}{4\mu}(x-y_k)^2\right]. \tag{4.27}$$

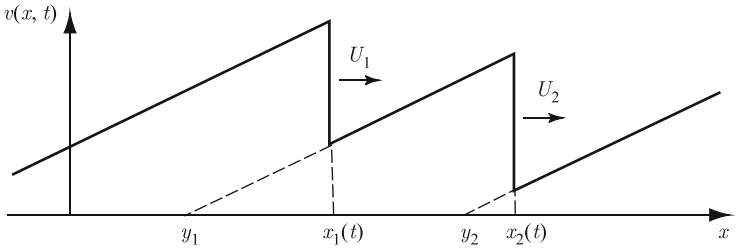

Fig. 4.5 Skeleton of a sawtooth wave. "Zeros" of the linear intervals and the coordinates of discontinuities are shown.

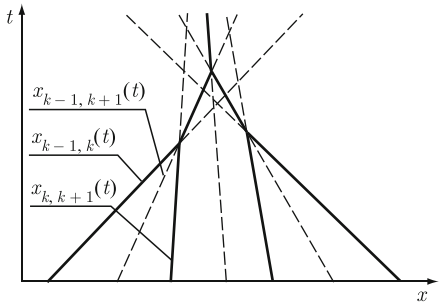

Fig. 4.6 Pattern of trajectories of coalescing shocks. Solid lines denote the trajectories of actually existing shocks.

Here

$$s_k = \sigma(y_k), \quad \sigma(x) = \frac{\partial^2 s_0(x)}{\partial x^2} = \frac{\partial v_0(x)}{\partial x}. \tag{4.28}$$

In the following, we assume that there is such ε that for for all k the following inequality holds:

$$\sigma_k > \varepsilon > 0.$$

By substituting (4.27) in (3.80), we find the solution of the linear diffusion equation

$$\varphi^k(x,t) = \frac{1}{\sqrt{1+\sigma_k t}} \exp\left[-\frac{\sigma_k t}{1+\sigma_k t}\frac{(x-y_k)^2}{4\mu t}\right]. \tag{4.29}$$

In the region

$$\varepsilon t \gg 1, \quad |x-y_k| \ll 2\sqrt{\varepsilon\mu}t, \tag{4.30}$$

the function $\varphi^k(x,t)$ (4.29) practically does not change, if we replace the right-hand side of the relationship (4.27) by the delta function:

$$\varphi_0^k(x) \sim \sqrt{\frac{4\pi\mu}{\sigma_k}} \exp\left(-\frac{s_k}{2\mu}\right) \delta(x-y_k).$$

By combining the contributions of all minimum points of the initial potential and taking into account the fact that the initial potential is defined up to an arbitrary constant factor, we arrive at the following assertion: *if the conditions* (4.30)

are satisfied, the solution of the Burgers equation is described by the expression (3.76), *where* $\varphi(x,t)$ *is the solution of the linear Burgers equation with initial condition* (4.20), *and*

$$Q_k = \frac{1}{\sqrt{\sigma_k}} \exp\left(-\frac{s_k}{2\mu}\right).$$

The factor in front of the exponential can be interpreted as a small correction to s_k:

$$\frac{1}{\sqrt{\sigma_k}} \exp\left(-\frac{s_k}{2\mu}\right) = \exp\left(-\frac{s'_k}{2\mu}\right), \quad s'_k = S_k + \frac{\mu}{2} \ln \sigma_k,$$

which, at small μ, can be neglected. As a result, we arrive at the initial condition (4.20), (4.21).

4.1.5 Periodic waves

In applied problems, for instance in nonlinear acoustics, evolution of periodic waves is of greatest interest. Therefore we devote some attention to the features of the solution of the Burgers equation with periodic initial conditions by examining them in the approximation of sawtooth waves.

First of all, let us discuss behavior of an initially harmonic field with the initial condition

$$v_0(x) = a \sin(\kappa x) \Rightarrow s_0(x) = -\frac{a}{\kappa} \cos(\kappa x). \tag{4.31}$$

Let us determine the condition of applicability of the sawtooth-wave approximation in relation to the originally harmonic wave. The characteristic curvature of the minimum points of the initial potential is here the same and equal to

$$\sigma_k = \varepsilon = a\kappa = \frac{1}{t_n}, \quad t_n = \frac{1}{a\kappa},$$

where t_n is the moment of shock formation. Apart from this, since the relative, and not absolute, values of the terms in the expression (4.23) are important, it is possible to rewrite the conditions (4.30) in the following form:

$$t \gg t_n, \quad \ell \ll \sqrt{\frac{\mu}{t_n}}\, t \quad \left(\ell = \frac{\pi}{\kappa}\right). \tag{4.32}$$

Let us find the sawtooth wave corresponding to the harmonic initial field (4.31). Since the minima of $s_0(x)$ within each period are the same, the values s_k in (4.23) can be assigned to be equal to zero. In addition to that, $y_k = 2\pi k/\kappa$. As a result, the expression for the sawtooth wave approximating the initially harmonic field assumes the following form:

$$v(x,y) = \frac{a}{\tau}\left(z - 2\pi \frac{\sum\limits_k k \exp\left[-\frac{\mathrm{R}}{8\tau}(z-2\pi k)^2\right]}{\sum\limits_k \exp\left[-\frac{\mathrm{R}}{8\tau}(z-2\pi k)^2\right]}\right). \tag{4.33}$$

Here we used the following notation:

$$z = \kappa x, \quad \tau = a\kappa t, \quad \mathrm{R} = \frac{2a}{\mu\kappa}. \tag{4.34}$$

The field $v(x,t)$ (4.33) for different values of τ are plotted in Fig. 4.7.

We also note that, at a large Reynolds number $\mathrm{R} \gg 1$, the conditions of applicability of the sawtooth-wave approximation (4.32) are reduced to the following inequality:

$$t \gg t_n\sqrt{\mathrm{R}}.$$

Let us discuss how the Reynolds number of the initial harmonic wave changes with time. If $\mathrm{R} \gg 1$, then there are three clearly distinct evolution stages of the field $v(x,t)$. At times

$$t < t_n$$

shocks are as yet absent, and the Reynolds number is close to its inititial value:

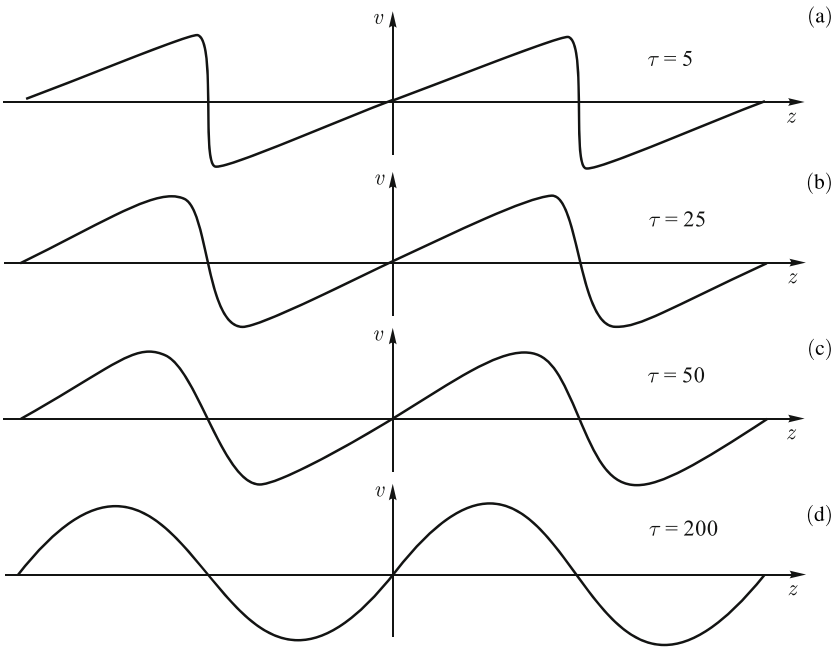

Fig. 4.7 Sawtooth wave (4.33) at $\mathrm{R} = 100$. The vertical scales of the plots are chosen so that the shape of the field $v(x,t)$ is clearly seen. It is seen that, with growing τ, the shocks get smeared out, and the field acquires a more and more sinusoidal profile, characteristic of the linear stage of evolution.

$$\mathrm{R}(t) \simeq \frac{a\ell}{\mu} = \frac{\pi a}{\mu\kappa} \simeq \mathrm{R} \quad (\ell = \frac{\pi}{\kappa}).$$

At $t \gg t_n$, the shock magnitude $U(t)$ and width $\delta(t)$ vary according to the laws

$$U(t) \simeq \frac{\ell}{t}, \quad \delta(t) \simeq \frac{2\mu}{U(t)},$$

and the Reynolds number decreases as $1/t$:

$$\mathrm{R}(t) \simeq \frac{U(t)\ell}{\mu} \simeq \frac{\ell^2}{\mu t}.$$

Finally, at $t \gtrsim t_l$, where t_l is the time at which the shock width becomes equal to the half-period of the field $v(x,t)$:

$$\delta(t_l) \simeq \ell \Rightarrow t_l \simeq \frac{\pi^2}{2\mu\kappa^2} \simeq \mathrm{R}\, t_n,$$

the linear stage sets in, and the Reynolds number tends to zero. A semi-qualitative graph of the current Reynolds number $\mathrm{R}(t)$ of the initially harmonic field $v(x,t)$ is depicted in Fig. 4.8.

Note. Let us note that the sawtooth wave, into which the initially harmonic field turns at $\mathrm{R} \gg 1$, possesses features of both N- and U-waves. Since the dissipation mechanism of N-waves is much more effective, the evolution of an initially harmonic wave and its approach to the linear stage develop according to the scenario of N-waves.

Let us also pay attention to the fact that the expression (4.33) does not contain information on the harmonicity of the initial field. The latter means that if a periodic field originally consists of several harmonic fields, then its asymptotic is determined by the wave with the largest period. Apart from that, the "final victory" of the large-scale component may be accelerated by the coalescence of shocks corresponding to a wave with a smaller period. The above-said illustrates the graphs of the solution of the Burgers equation, shown in Fig. 4.9, with the initial condition

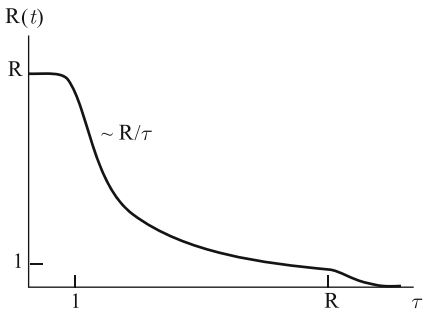

Fig. 4.8 Semi-qualitative graph of the current Reynolds number of a periodic field at a large initial Reynolds number $\mathrm{R} \gg 1$ as a function of the dimensionless time $\tau = a\kappa t$.

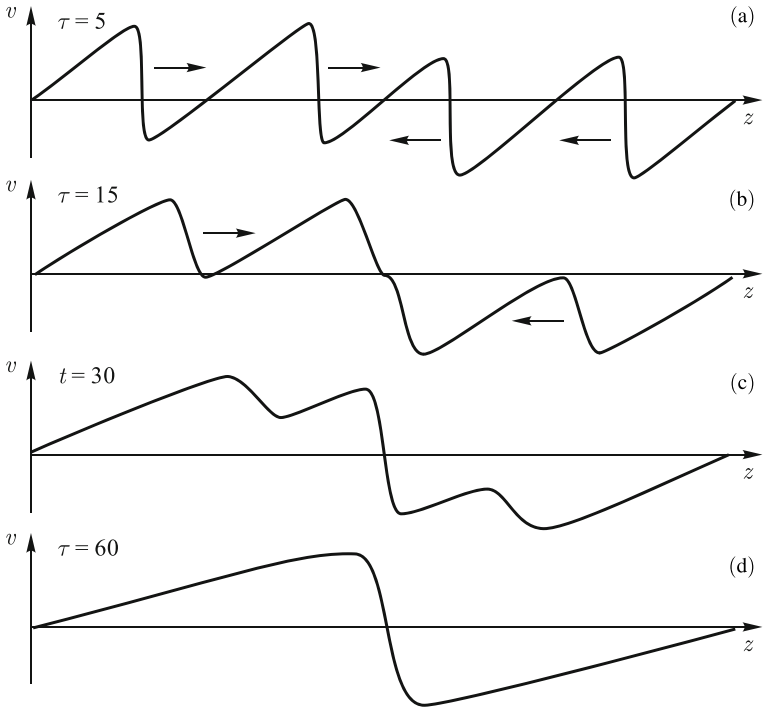

Fig. 4.9 Evolution of the solution to the Burgers equation with the initial condition (4.35) and R = 50. It is seen that the coalescence of shocks leads to the formation of a sawtooth wave with the period of the large-scale component of the initial condition.

$$v_0(x) = a\left[\sin(\kappa x) + \tfrac{1}{4}\sin\left(\tfrac{1}{4}\kappa x\right)\right] \tag{4.35}$$

at R = 50. The definition of the initial Reynolds number and other dimensionless parameters is borrowed from (4.34).

From this figure, it is seen that first shock corresponding to the small-scale component of the initial condition (4.35) are formed. Then, due to modulation of shock velocities of the large-scale component, the shocks coalesce, forming, in the end, one shock per period of the large-scale component of the initial condition.

4.2 Evolution of complex signals

In this section, we discuss several examples of evolution of complex signals having not one, but a set of characteristic length scales. Their behavior may qualitatively differ from evolution of single-scale signals. So it is conventional to believe that dissipation leads to a relative decrease of the role of nonlinear effects, and the nonlinear stage of evolution is succeeded by the linear stage. But the reverse sequence

of events is possible, when the linear stage of evolution precedes the the nonlinear one. Let, for instance, the initial field have the form of a sequence of N spaced pulses with the initial Reynolds number $\mathrm{R}_0 \ll 1$. Because of linear diffusion, the pulses spread out, assume a Gaussian shape, and then merge into a single pulse with the Reynolds number $\mathrm{R}(t) = N\mathrm{R}_0$. If thereby $\mathrm{R}(t) \gg 1$, then the subsequent evolution has a pronounced nonlinear character. Below we discuss other characteristic examples of complex signal evolution.

4.2.1 Quasiperiodic complex signals

Let us illustrate, in detail, a possible "anomalous" behavior of complex signals consisting in that their effective current Reynolds number may not only decrease or stay constant, but also grow with time. We do so by discussing the behavior of periodic and quasiperiodic fields as an example.

Let the initial field equal the sum of the harmonic components:

$$v_0(x) = a\left[\sin(\kappa x) + \beta^{\gamma-1}\sin(\beta\kappa x)\right] \quad (\beta \ll 1). \tag{4.36}$$

Let us introduce, in analogy with the way it has been done above, the characteristic times of nonlinearity and approach to the linear regime for the second harmonic term. They are equal to

$$t_n(\beta) \simeq \beta^{-\gamma} t_n, \quad t_l(\beta) \simeq \beta^{-2} t_l \simeq \beta^{-2}\mathrm{R}\, t_n.$$

If the following inequality holds:

$$t_l \lesssim t_n(\beta) \Rightarrow \mathrm{R}\,\beta^{\gamma} \lesssim 1 \Rightarrow \gamma > 0,$$

then, at $t < t_l$, the second term has practically no influence on the evolution of the shape of the first periodic wave, and by the moment of time $t \gtrsim t_l$, which it practically completely dissipates, the resultant field is approximately equal to

$$v(x, t \gtrsim t_l) \simeq a\,\beta^{\gamma-1}\sin(\beta\kappa x).$$

Its Reynolds number is:

$$\mathrm{R}(t_n(\beta)) \simeq \frac{t_l(\beta)}{t_n(\beta)} \simeq \mathrm{R}\,\beta^{\gamma-2}.$$

Thus, when the condition

$$0 < \gamma < 2 \tag{4.37}$$

holds, the Reynolds number by the beginning of the nonlinear stage of development of the large-scale component in (4.36) becomes greater than the initial Reynolds number.

Let us consider a more complex quasiperiodic initial field

$$v_0(x) = a \sum_{k=1}^{\infty} \beta^{(\gamma-1)k} \sin(\beta^k \kappa x + \theta_k), \tag{4.38}$$

where θ_k are arbitrary phase shifts. If the above-listed limitations of β hold, and γ satisfies the inequalities (4.37), then by the moment of time

$$t^k \simeq \beta^{-k\gamma} t_n$$

the nonlinear stage for the kth term of the sum (4.38) sets in, the previous terms have been eliminated due to dissipation, and the next ones produce a quasi-constant background. Accordingly, the current Reynolds number is equal to

$$\mathrm{R}(t^k) \simeq \mathrm{R}\,\beta^{k(\gamma-2)}.$$

By eliminating β from the two latter inequalities, we find that, when the condition (4.37) holds, the Reynolds number, on average, grows with time without limit according to the power law

$$\mathrm{R}(t) \simeq \mathrm{R}\left(\frac{t}{t_n}\right)^{(2-\gamma)/\gamma}.$$

4.2.2 Evolution of fractal signals

Behavior of fields qualitatively changes even more for complex signals having a fractal structure [3].

Let, e.g., there exist N unidirectional pulses with the period L_1 and this structure is reproduced N times with the period $L_2 = \beta L_1$. Then the number of pulses within the specified length scale is equal to N^2. Let this procedure be repeated M times, whereas $L_i = \beta L_{i-1}$, $\beta = (N-1)\gamma$ and $\gamma > 1$. Within the length scale L_M, the pulse duration is equal to $T_M = L_M(N-1)$, and the number of pulses in the sequence is equal to N^M. At $M \gg 1$, it is possible to introduce the fractal dimension of such a signal as $D = \lim(\ln R/\ln L)$, where $R = N^i$ is the number of pulses within the interval $L = L_1 N \beta^{i-1}$ and

$$D = \ln N/\ln[(N-1)\gamma].$$

If $(N-1)\gamma = N$, then $D = 1$ and we have a periodic signal with the period L_1. But if the external period $T_M = 1$, and $M \to \infty$, then it is easy to see that the sequence of the pulse coordinates forms a Cantor set. So, if $N = 2$, $\beta = 3$, then $D = \ln 2/\ln 3$. Illustration of Cantor set signal evolution is depicted, schematically, in Fig. 4.10.

Let us discuss evolution of a signal at the smallest scale L_1. The Reynolds number of a single pulse is equal to $\mathrm{R}_0 = m/2\mu$, and if $\mathrm{R}_0 \ll 1$, then we have the linear stage

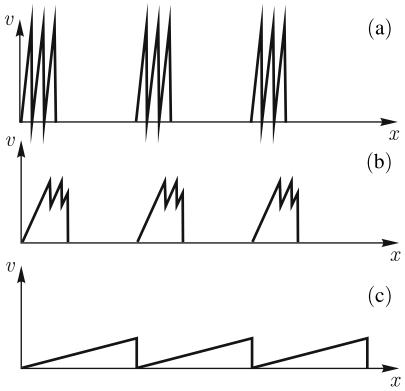

Fig. 4.10 Evolution of a Cantor set.

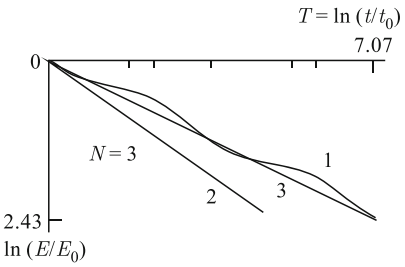

Fig. 4.11 Energy decay of the Cantor set (curve 1), decay of a single pulse (curve 2), average law of decay (curve 3).

of decay, where the width of each pulse grows as $l(t) = (2\mu t)^{1/2}$. At times, when $l(t) \gg L_1 N$, the sequence of N pulses, due to *linear diffusion*, will turn into a single pulse with the Reynolds number $\mathrm{R}_1 = mN/2\mu = N\mathrm{R}_0 > \mathrm{R}_0$. Thus, because of linear diffusion, the Reynolds number grows, the linear stage is eventually succeeded by the nonlinear one, and we can limit ourselves to an analysis in the limit of $\mu \to 0$. At the smallest scale, each separate pulse turns into a triangular one of length $x_s(t) = (2mt)^{1/2}$, and its energy decays as $E(t) = x_s^3/3t^2 = (2m)^{3/2}t^{1/2}$. Interaction between pulses starts at $t > t_0$, where $t_0 = L_1^2/2m$ is determined from the condition $x_s(t) = L_1$. After coalescence of all shocks at the smallest scale, the N pulses turn into a single triangular pulse of length $x_s(t) = (2Nmt)^{1/2}$, and its energy is $N^{1/2}$ times greater than the energy of N noninteracting pulses. At the moment of time $t_1 = L_2 N^2/2m = t_0\beta^2/N$, coalescence of pulses at the second scale begins. As a result, the field's evolution is logarithmically self-similar, i.e. within the time interval $t \in [t_0(\beta^2/N)^i, t_0(\beta^2/N)^{i+1}]$, the field reproduces the evolution within the interval $t \in [t_0, t_0\beta^2/N]$. The average law of energy decay is thereby determined by the signal's fractal dimension D:

$$E(t) = C_E(t/t_0)^{-p}, \quad p = (1-D)/(2-D), \quad 0 < p < 1/2.$$

In Ref. [4], spectral, diffusive and convective properties of one-dimensional homogeneous fractal non-alternating pulse fields displaying a well-defined Kolmogorov capacity D was investigated. The energy spectrum of fractal or spiral al-

ternating pulse fields scales as k^D. The energy spectrum of scales as k^D. Both these scaling laws hold in a range of wavenumbers between η^{-1} and L^{-1}, where η is the smallest distance between pulses and $L(\gg \eta)$ is a characteristic large scale of the structure. The space-filling geometry, which is quantified by the Kolmogorov capacity D, makes the field less autocorrelated (more singular) in the alternating case, whereas it makes it more autocorrelated (less singular) in the non-alternating case. For homogeneous fractal non-alternating pulse fields energy decays also as

$$E(t) = C_E(t/t_0)^{-p}, \quad p = (1-D)/(2-D).$$

4.2.3 Evolution of multi-scale signals — a dynamic turbulence model

Analysis of the so-called Burgers turbulence is an important example of evolution of complex signals. It is a common convention to call evolution of random fields satisfying the Burgers equation "the Burgers turbulence" (see, e.g., [5–8]). In the case of vanishingly small viscosity, a continuous field is transformed into a random sawtooth wave, i.e. a sequence of triangular pulses with the same slope $\partial_x v = 1/t$ and with random positions of shocks. Due to multiple coalescence of shocks, statistical properties of such a random field become self-similar and are characterized by the only integral length scale $L(t)$. Because of the coalescence of shocks, the integral length scale grows, which causes the energy of the turbulence

$$\sigma^2(t) \sim L^2(t)/t^2 \tag{4.39}$$

to decay at a slower rate than the energy of a periodic signal. The evolution type of the turbulence is determined by the behavior of large-scale components of the initial energy spectrum

$$E_0(k) = \alpha^2 k^n b_0(k); \tag{4.40}$$

$$E_0(k) = \frac{1}{2\pi}\int \langle v_0(x), v_0(x+z)\rangle e^{ikz} dz. \tag{4.41}$$

Here $b_0(k)$ is a function, which decays sufficiently rapidly at $k > k_0 \sim l_0^{-1}$, and $b_0(0) = 1$. We also note that the angular brackets $\langle \cdots \rangle$ here and in the following denote statistical averaging.

At $n < 1$, the integral scale of the turbulence $L(t)$ grows as

$$L(t) = (\alpha t)^{2/(3+n)}. \tag{4.42}$$

(see, e.g., [9]). From (4.39), for the energy of the turbulence, we thereby have:

$$\sigma^2(t) \sim t^{-p}, \; p = \frac{2(n+1)}{n+3}. \tag{4.43}$$

Let us also discuss the example of the damping of a *multiscale* deterministic signal with an initial discrete spectrum, whose average properties (the integral length scale and energy) are similar to the decay laws of the Burgers turbulence with a continuous initial spectrum [10].

Let the initial field have the following form:

$$v_0(x) = \sum_{p=0}^{\infty} a_p A_{inv}(k_p x + \phi_p). \tag{4.44}$$

Here a_p, k_p are the amplitude and wavenumber of a mode, and ϕ_p is its phase. We assume that the spatial frequencies of modes k_p form a Weierstrass spectrum (accumulate towards the zero frequency), and their amplitudes are chosen from the condition $a_p^2 = E_0(k_p)\Delta_p$, $E_0(k) \sim k^n$, where $E_0(k)$ is the energy spectrum of the continuous signal

$$k_p = k_0 \varepsilon^p, \quad a_p = a_0 \varepsilon^{-hp}, \quad h = -\frac{n+1}{2}, \quad a_0 = \alpha k_0^{(n+1)/2}. \tag{4.45}$$

Here h is a similarity parameter.

We choose the modes to be of the form of the following 2π-periodic inverse sawtooth function $A_{inv}(x)$,

$$A(x) = \pi - x, \quad x \in [0, 2\pi) \tag{4.46}$$

whose feature is the formation of a finite-amplitude shock.

4.2.3.1 Evolution and interaction of inverse sawtooth modes

As it was shown above, the solution of the Burgers equation with the initial linear profile $v_0 = -\gamma(x - x_+)$ has the following form:

$$v(x,t) = \frac{-\gamma(x - x_+)}{1 - \gamma t}.$$

The quantity γ^{-1} has the dimension of time, and, for $\gamma > 0$ during a finite time period $t = \gamma^{-1}$, the gradient $\partial_x v$ becomes infinite. For $\gamma < 0$, the gradient becomes equal to $\partial_x v = t^{-1}$, regardless of the initial gradient γ, at times $t \gg |\gamma|^{-1}$. Thus, from the previous relationships, we have that the evolution of the pth mode is characterized by the nonlinear time

$$t_p = \gamma_p^{-1} = a_p {k_p}^{-1} = t_0 / (\varepsilon^{(n+3)/2})^p, \quad t_0 = 1/\alpha k_0^{n+3/2}. \tag{4.47}$$

From the solution (3.21), it is easy to see that, at the moment of time $t = t_p$, the pth mode is transformed into an "ordinary" sawtooth wave with the slope $\partial_x v = 1/t$ independent of the amplitude and wavenumber of this mode. Thereby, the energy

density of this mode $\sigma^2(t) = \langle v^2(x,t)\rangle_L$, where $\langle\cdots\rangle_L$ denotes averaging over the period, is conserved at $t < t_p$ and decays as $(k_p t)^{-2}$ at $t > t_p$.

As it was shown in Sect. 4.1.4, evolution of the velocity field in the Burgers equation at $\mu \to 0$ is equivalent to evolution of a gas of coalescing particles with a constant initial velocity. For the pth mode at the initial stage, for the density, we have

$$\rho(x,t) = \rho_0 \frac{1}{1 - t/t_p}, \quad \left| \frac{\pi}{k_p} - x \right| < \frac{t}{t_p} \frac{\pi}{k_p}, \tag{4.48}$$

and ρ is equal to zero outside this interval. At the moment of time $t = t_p$, all light particles merge into a heavy particle of a mass

$$m_p = \rho_0 L_p = \rho_0 \frac{2\pi}{k_p}, \tag{4.49}$$

with the coordinate

$$x_{p,l} = \frac{\pi}{k_p} - \frac{\phi_p}{k_p} + \frac{2\pi}{k_p} l; \quad l = 0, \pm 1, \pm 2, \ldots \tag{4.50}$$

equivalent to the zero of the pth mode. The process of the velocity evolution and of the coalescence of particles is depicted in Fig. 4.12.

Let us now consider interaction of two adjacent modes, the pth and $(p+1)$th. From Eq. (4.47), it is seen that the ratio of nonlinear times of these consecutive modes is equal to

$$\frac{t_{p+1}}{t_p} = \varepsilon^{-(n+3)/2} \equiv \varepsilon^{1-h} \tag{4.51}$$

and does not depend on p. The gradient of the initial field $v_{(p)}(x) + v_{(p+1)}(x)$ is equal to $-(\gamma_p + \gamma_{p+1})$, and the effective nonlinear time of this field is

$$t_{p,\text{eff}} = t_{p,p+1} = \frac{1}{\gamma_p + \gamma_{p+1}} = \frac{t_p}{1 + t_p/t_{p+1}}. \tag{4.52}$$

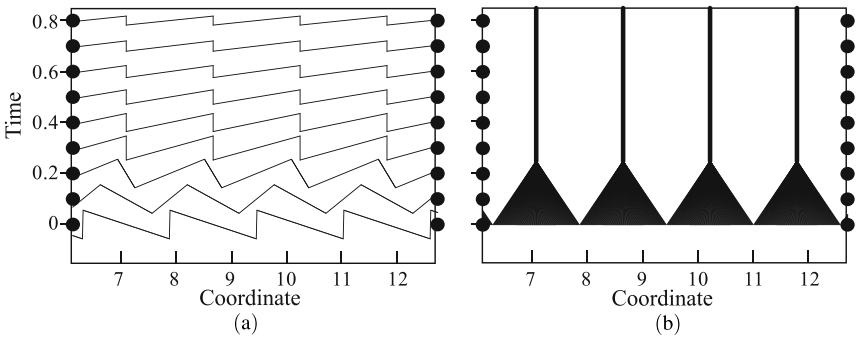

Fig. 4.12 Evolution of an inverse mode and coalescence of light particles into clusters.

Thus the large-scale mode leads to a faster appearance of shocks in the small-scale mode. Since the initial gradient is the same for all points of the initial profile, all light particles coalesce at the same time $t = t_{p,p+1}$. Suppose the following relationship between the phases of the consecutive modes holds:

$$k_{p+1}\phi_{p+1} = k_p\phi_p + 2\pi r/N. \tag{4.53}$$

In this case, the shocks of the low-frequency $(p+1)$th mode lead to appearance of additional shocks in the total field $v_{(p)}(x) + v_{(p+1)}(x)$ compared with the pth mode. Thus, at times $t > t_{r,\text{eff}}$, the masses of all heavy particles will be the same as in the absence of the large-scale mode.

The coordinates of these particles at the moment of time $t = t_{p,\text{eff}}$ are equal to

$$X_{(p,l)}(t_{p,\text{eff}}) = x_{p,l} + v_{(p+1)}(x_{p,l})t_{p,\text{eff}}, \tag{4.54}$$

where $x_{p,l}$ are the positions of the zeros of the pth mode (4.50). The velocity of these particles is equal to $v_{(p+1)}(x_{p,l})$. Eq. (4.54) becomes obvious if we use the trivial equality $v_{(p)}(x_{p,l}) + v_{(p+1)}(x_{p,l}) = v_{(p+1)}(x_{p,l})$. From Eq. (4.54) we immediately have that at times greater than $t_{p,\text{eff}}$, the coordinates of heavy particles behave as

$$X_{(p,l)}(t) = x_{(p,l)} + v_{(p+1)}(x_{p,l})t. \tag{4.55}$$

The distance between consecutive heavy particles $X_{p,l}(t)$ and $X_{p,l+1}(t)$ decreases with time proportionally to the initial gradient of the large-scale mode $v_{(p+1)}(x)$:

$$\begin{aligned} X_{p,l+1}(t) - X_{p,l}(t) &= (x_{p,l+1} - x_{p,l}) - t\frac{\partial v_{(p+1)}(x)}{\partial x}(x_{p,l+1} - x_{p,l}) \\ &\equiv (x_{p,l+1} - x_{p,l})(1 - t/t_{p+1}). \end{aligned} \tag{4.56}$$

From here it is seen that at the moment of time $t = t_{p+1}$ these particles coalesce, and the newly merged particles have have the masses

$$m_{(p+1)} = \rho_0 L_{p+1} \tag{4.57}$$

and coordinates

$$x_{p+1,l} = \frac{\pi}{k_{p+1}} - \frac{\phi_{p+1}}{k_p} + \frac{2\pi l}{k_{p+1}}; \quad l = 0, \pm 1, \pm 2, \ldots \tag{4.58}$$

Their velocities are equal to zero.

Thus, if t is greater than t_{p+1}, the evolution of the initial excitation $v_0(x) = v_{(p)}(x) + v_{(p+1)}(x)$ is the same as the evolution of only one large-scale mode $v_{(p+1)}(x)$. Evolution of the velocity field of two consecutive modes and the corresponding process of particle coalescence are depicted in Fig. 4.13.

It is evident that under a suitable choice of the wavenumbers $k_p = k_0/N^p$ and phases of modes and for a finite total $v(x) = v_{(p)}(x) + v_{(p+1)}(x) + \ldots + v_{(M)}(x)$, the evolution of the field at long times greater than t_M will be the same as the evolution

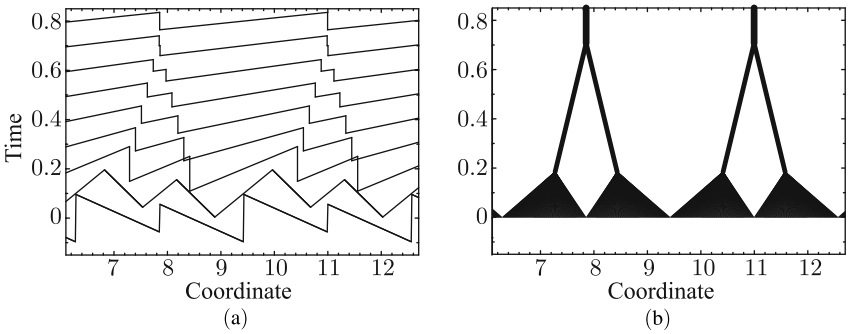

Fig. 4.13 Interaction of two consecutive inverse modes and coalescence of light particles into clusters.

of the only large-scale mode $v_{(M)}(x)$. For integral N, the minimum combination frequency of all interacting harmonics is equal to the wavenumber of the largest mode $k_M = k_0/N^M$. Hence nonlinear interaction does not lead to generation of new components with wavenumbers less than k_M.

4.2.3.2 Interaction of a small-scale inverse sawtooth mode with a large-scale structure

Let us consider interaction of the pth small-scale mode with the field in the form of an infinite series of large-scale modes

$$W_p(x) = \sum_{r=p+1}^{\infty} v_r(x) \equiv \sum_{r=p+1}^{\infty} a_r A(k_r x + \phi_r), \tag{4.59}$$

assuming that the phases of these modes satisfy the condition (4.53), and for the wavenumbers, as before, the relationship $k_r = k_0 \varepsilon^r,\ a_r = a_0 \varepsilon^{-hr},\ h = -(n+1)/2$ holds. The interaction process can, thereby, be conveniently interpreted in terms of particles. From (4.59) and (4.47) for the gradient of the initial excitation $v_0(x) = v_p(x) + W_p(x)$ we have

$$\begin{aligned} \frac{\partial v_0(x)}{\partial x} &= \frac{\partial v_p(x)}{\partial x} + \frac{\partial W_p(x)}{\partial x} = \sum_{r=p}^{\infty} \gamma_p \\ &= \gamma_0 \sum_{r=p}^{\infty} (\varepsilon^{\frac{(n+3)}{2}})^r = \gamma_0 \varepsilon^{\frac{(n+3)}{2} p} \frac{1}{1 - \varepsilon^{\frac{(n+3)}{2}}}. \end{aligned} \tag{4.60}$$

For convergence of the series, it is here assumed that $n > -3$ ($h < 1$). From this equation follows that the effective nonlinearity time of the pth mode is equal to

$$\tilde{t}_p = \left(\frac{\partial v_0(x)}{\partial x} \right)^{-1} = t_p \left(1 - \varepsilon^{\frac{(n+3)}{2}} \right), \tag{4.61}$$

where t_p is determined by Eq. (4.47).

Thus, at the moment of time $\tilde{t}_p$, light particles coalesce into heavy ones of a mass $m_p = \rho_0 L_p$ (4.57). Coordinates of these particles are determined by the equation analogous to Eq. (4.55):

$$x_{p,l}(t) = x_{p,l}(t) + W_p(x_{p,l})t, \tag{4.62}$$

where the particle velocities are determined by the function $W_p(x)$ (4.59), which represents an infinite sum of large-scale modes, and $x_{p,l}$ are the coordinates of the zeros of the pth mode.

The distance between the coordinates of two adjacent heavy particles $x_{p,l}$ and $x_{p,l}$ decreases with time as $(1 - t/\tilde{t}_{p+1})$, where $\tilde{t}_{p+1} = t_{p+1}(1 - \varepsilon^{(n+3)/2})$ is the reciprocal of the gradient of the function $W_p(x)$, (see relationships (4.59) and (4.60)). Hence the time of coalescence of particles of this generation is determined by Eq. (4.61) with $p = p + 1$, and the masses of new particles will be determined by the period of the $(p+1)$th — see Eq. (4.57).

Extrapolation of the process of heavy particle coalescence in the following generations is obvious. Particle collision in the qth generation takes place at the moment of time $\tilde{t}_{p+q} = t_{p+q}(1 - \varepsilon^{\frac{n+3}{2}})$, and the masses of these particles at this moment of time are determined by the period of the $(p+q)$th mode $m_{p+q} = \rho_0 L_{p+q} = 2\pi\rho_0/k_{p+q}$. During the interval between collisions $t \in [\tilde{t}_{p+q}, \tilde{t}_{p+q+1}]$

$$\frac{\tilde{t}_{p+q+1}}{\tilde{t}_{p+q}} = \varepsilon^{-\frac{(n+3)}{2}} = N^{\frac{n+3}{2}}, \tag{4.63}$$

the particle coordinates will be determined by Eq. (4.62) with $p = p + q$. Here $W_{p+q}(x)$ is the sum of velocities of all large-scale modes with $r > p + q$, and $x_{p+q,l}$ are the zeros of the $(p+q)$th mode. It is important to emphasize that, at $t > \tilde{t}_{p+q}$, the evolution of particles is completely determined only by large-scale modes with $r \geqslant p + q$. This means that, at times $t > \tilde{t}_{p+q}$, the particle positions do not depend on the presence of small-scale excitations with $r < p + q$ in the initial excitation.

Thus, for two different initial velocities: a field with small-scale modes $\tilde{v}_0(x)$ and a field without smal-scale modes $v_0(x)$:

$$v_0(x) = W_{p+q-1}(x); \;\; \tilde{v}_0(x) = W_{p-1}(x) \tag{4.64}$$

the fields will be the same at $t > \tilde{t}_{p+q-1}$. Even if $p \to -\infty$ (when in the initial excitation there are modes with very small scales $L_p \sim \varepsilon^{-p} = N^p$ and very large amplitudes $a_p \sim a_0(\varepsilon^{(n+1)/2})^p = a_0(N^{(n+1)/2})^{-p})$ multiple coalescence of particles leads to independent evolution of large-scale excitations with respect to small-scale modes.

This effect is similar to the effect of self-preservation of large-scale structures in the Burgers turbulence [11–13]. If the initial excitation $v_0(x)$ represents a noise

field, then multiple coalescence of shocks leads to continuous growth of the integral length scale of the turbulence $L(t)$. In the presence of small-scale perturbations $v_h(x)$, the shock coordinates of the large-scale structure will deviate from unperturbed positions, and these deviations $\Delta x_k(t)$ grow with time. Thus evolution of large-scale structures is determined by competition of two factors: the growth of the integral length scale $L(t)$ due to coalescence of large-scale shocks and the growth of deviations of shock positions $\Delta x_k(t)$ from the unperturbed value because of the presence of small-scale perturbations $v_h(x)$. For the Burgers turbulence having the energy spectrum (4.40) with $n < 1$, multiple coalescence of shocks leads to stability of large-scale structures with respect to small-scale perturbations. For the model signal considered above, this effect occurs for arbitrary n due to a special choice of the wavenumbers and phases of the interacting modes.

As it has been mentioned several times, the evolution of the velocity field in the Burgers equation has a one-to-one correspondence with the evolution of a gas of coalescing particles. At the stage, when all light particles merged into heavy ones, the gradient of the velocity field at all points of space is the same $\partial_x v = 1/t$. At this stage, the profile of the field $v(x,t)$ is completely determined by the coordinates and velocities of heavy particles. Their coordinates coincide with the shock coordinates $X_s(t)$, and the shock velocities satisfy the well-known relationship

$$v_s(t) = \frac{dX_s(t)}{dt} = \frac{v_s(x_s - 0,t) + v_s(x_s + 0,t)}{2} \tag{4.65}$$

and are equal to the velocity of heavy particles. The shock amplitudes

$$\Delta v_s(x) = v(x_s - 0,t) - v(x_s + 0,t) = \frac{m}{t} \tag{4.66}$$

are determined by the mass of heavy particles ($\rho_0 \equiv 1$).

Thus the investigation of heavy particle motion allows us completely to reconstruct the velocity field $v(x,t)$ of the Burgers equation.

4.2.3.3 Weierstrass-Mandelbrot sawtooth function

As is has been shown above, evolution of heavy particles (shocks) is determined by the function $W_p(x)$ (4.59). The base functions $W_p(x)$ are the periodic inverse sawtooth functions with the wavenumbers $k_r = k_0\varepsilon^r$ and amplitudes $a_r = a_0\varepsilon^{-hr}$, $h = -(n+1)/2$. The wavenumbers form a geometric progression as in the Weierstrass function (see, e.g., [14]), and accumulate toward the point $k = 0$.

In the standard Weierstrass function, the situation is the opposite, i.e. its frequencies continuously grow. Nevertheless, the function $W_p(x)$ possesses many properties of the Weierstrass function and of its generalization, viz. the Weierstrass-Mandelbrot function (see [14, 15]).

Here we consider a deterministic function $W_p(x)$ with special phase relations between mode phases $\phi_p = (2\pi k/N)p$ ($k = 1,2,\ldots,N; N = 1/\varepsilon$), so that shocks of

the large-scale modes $r > p+1$ coincide with some of the shocks of the small-scale mode $r = p+1$. The function $W_p(x)$ is continuous within the intervals $2\pi/k_{p+1} = 2\pi/(k_0\varepsilon^{p+1})$ and has there the same slope (gradient). The reciprocal of this gradient has the dimension of time $\tilde{t}_{p+1}$

$$\tilde{t}_{p+1} = t_{p+1}(1-\varepsilon^{\frac{n+3}{2}}); \quad t_{p+1} = t_0(\varepsilon^{\frac{n+3}{2}})^{p+1} \tag{4.67}$$

and is proportional to the nonlinearity time t_{p+1} of the smallest-scale mode. Evidently, we assume that $n > -3$, which guarantees convergence of (4.60) and validity of the inequality $t_{p+1} > t_p$. The amplitudes of modes are proportional to $\varepsilon^{(n+1)/2}$ and at $n > -1$ the function $W_p(x)$ is bounded

$$W_p(x) \leqslant \sum_{r=p+1}^{\infty} a_r = a_0(\varepsilon^{\frac{n+1}{2}})^{p+1}\,\frac{1}{1-\varepsilon^{\frac{n+1}{2}}}. \tag{4.68}$$

Thus, at finite p, the energy of $W_p(x)$ is also finite. Thereby the function possesses scaling properties

$$W_p(x) = \varepsilon^{-hp}W_0(\varepsilon^p x); \quad W_p(\varepsilon^m x) = \varepsilon^{hm}W_{m+p}(x). \tag{4.69}$$

The case $-1 < n < 1$ is here equivalent to initial conditions for the Burgers turbulence in the form of white noise. The energy of the initial noise is thereby determined by the ultraviolet cutoff frequency, which in this model corresponds to the smallest length scale p. If $p \to -\infty$, the energy of the model signal (as well as the energy of white noise) tends to infinity. But, as it follows from the analysis given above, during a finite time due to nonlinear dissipation t, all modes with $t_p < t$ have a finite energy $\sim L_p^2/t^2$ and, thus, the total energy of the wave is also finite. Hence, even if there is divergence of initial conditions ($p \to -\infty$), there exist a solution with a finite energy for any time $t > 0$.

The case $n < -1$ is similar to the fractal Brownian motion for the velocity in the Burgers turbulence. The series (4.68) in this case diverges and the initial excitation $W_p(x)$ is unbounded. For the Burgers turbulence, however, here only relative motion of particles (shocks) is important. Thus it is possible to perform regularization of the function $W_p(x)$, similar to regularization of the Weierstrass function [15].

So, assuming that $\phi_p \equiv 0$, it is possible, according to [15], to introduce the function $W_p^{\infty}(x) = W_p(x) - W_p(0)$, bounded within any finite interval.

4.2.3.4 Self-similar properties of a multi-scale signal

By using the scaling characteristics of the Weierstrass-Mandelbrot function $W_p(x)$, let us show that its evolution in the framework of the Burgers equation is of a logarithmically periodic, self-similar character.

Let us discuss evolution of the multi-scale signal

$$v_0(x) = v_p(x) + W_p(x). \tag{4.70}$$

As it has been shown, at times $t > \tilde{t}_p$, all light particles coalesce and form heavy particles of a mass $M_p = \rho_0 L_p$, and their motion is determined by Eq. (4.63). These particles coalesce at the moment of time $\tilde{t}_{p+1}$, ($\tilde{t}_{p+1}/\tilde{t}_p = N^{\frac{(n+3)}{2}}, N = \varepsilon^{-1}$), and new heavy particles have the mass $m_{p+1} = \rho_0 L_{p+1} = m_p N$. Their motion is determined by the same laws (4.63), but with a change of the subscript of the Weierstrass-Mandelbrot function $p \to p+1$. By using the scaling properties of $W_p(x)$ (4.69) we have that the motion of particles in this time interval is similar to the motion of particles in the interval $[\tilde{t}_p, \tilde{t}_{p+1}]$, if renormalize time $t/\tilde{t}_p \Rightarrow t/\tilde{t}_{p+1}$. Since the ratio of the coalescence times t_{p+1}/t_p does not depend on p, we can speak about logarithmically periodic self-similarity of particle motion. This means that within an arbitrary time interval $[\tilde{t}_q, \tilde{t}_{q+1}]$, particle motion will be similar to motion of particles within the interval $\tilde{t}_p, \tilde{t}_{p+1}$, with similarity parameters $x_p/x_q = \varepsilon^{p-q}$ in the coordinate space and $t_p/t_q = (\varepsilon^{-\frac{n+3}{2}})^{p-q}$ in time. But since the coordinates and masses of particles completely determine the velocity field, then the solution of the Burgers equation with such initial conditions will also be logarithmically periodic self-similar.

After each collision, the mass of particles $M(t)$ increases $N = 1/\varepsilon$ times. The time intervals between consecutive collisions grow as $t_{p+1}/t_p = N^{\frac{n+3}{2}}$. Thus, by approximating the piecewise-constant function $m(t)$ by the power law

$$m(t) \simeq m_0 (t/t_0)^{(n+3)/2}, \tag{4.71}$$

we obtain the same law as the law of growth of the integral length scale $L(t) \sim m(t)$ for the Burgers turbulence.

For the case $n > -1$, it is also not difficult to estimate the law of decay of the energy of the model signal. At $n > -1$ and $\varepsilon \ll 1$, the main energy of the signal at the moment of time t is in the mode with the smallest period and it is proportional to $L^2(t)/t^2$. Thus, also for the averaged law of energy decay of the model signal we obtain the same law of energy decay as for the Burgers turbulence.

In order to illustrate evolution of model self-similar signals, we show the velocity profiles at different moments of time and trajectories of coalescing particles for initial conditions of the "white noise" ($n = 0$, $h = -1/2$) and "Brownian" motion ($n = -2$, $h = 1/2$) types. In experiments, ten modes have been taken with the ratio of the consecutive wavenumbers of $\varepsilon = 1/N = 1/2$. In Figs. 4.14, 4.15, the initial stage of evolution is depicted in a certain sufficiently small spatial interval, when the finiteness of the number of modes has not yet manifested itself.

From Fig. 4.14, it is seen that for $n = 0$ the initial sawtooth multi-scale function oscillates about $v = 0$ similarly to a "white noise" with a finite variance. After coalescence of light particles, when the "inverse" sawtooth function is transformed into a sawtooth wave with the same positive gradient $\partial_x v = 1/t$, the structure of the signal is relatively simple and, even at $N = 2$, the main energy is concentrated in the mode with the smallest wavenumber.

In the case $n = -2$, the initial profile has large deviations, which is typical of Brownian motion. After coalescence of light particles, the wave profile represents a

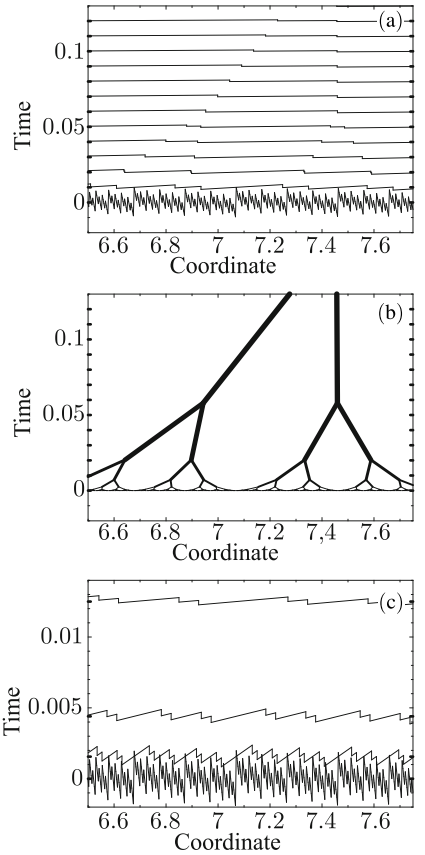

Fig. 4.14 Profile of the field **(a)** and trajectories of clusters (shocks) **(b)** for the initial conditions of the "white noise" type ($n = 0$, $h = -1/2$). In the last panel **(c)**, the profiles of the field at the moments of similarity are shown.

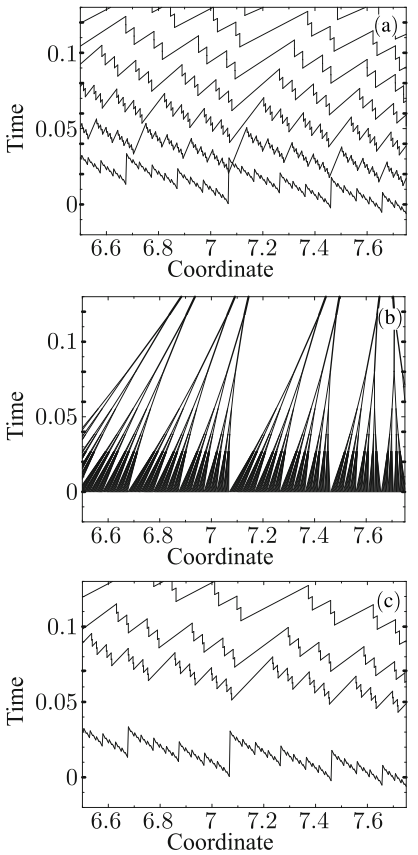

Fig. 4.15 Profile of the field **(a)** and trajectories of clusters (shocks) **(b)** for the initial conditions of the "Brownian motion" type ($n = -2$, $h = 1/2$). In the last panel **(c)**, the profiles of the field at the moments of similarity are shown.

sequence of shocks of different amplitude, which also imitates properties of Brownian motion in the Burgers turbulence [16].

In the latter graphs, the velocity profiles at three consecutive moments of coalescence of heavy particles $t_*/t_{**} = N^{(n+3)/2}$ are shown. These figures illustrate the logarithmically periodic self-similarity of evolution of multi-scale signals.

4.2.3.5 Evolution of multi-scale fields in the vector Burgers equation

The Burgers equation admits a generalization to the multidimensional case

$$\partial_t \mathbf{v} + (\mathbf{v}\cdot\nabla)\mathbf{v} = \mu\nabla^2\mathbf{v}.$$

Its detailed discussion is deferred until Chapter 6, where, in particular, it will be shown that for potential fields, it is also reduced to the linear diffusion equation. Its asymptotic solution at vanishing viscosity is completely analogous to the corresponding solution of the one-dimensional Burgers equation.

Here we only note that multi-scale solutions, similar to the ones considered above, can be constructed and for the vectorial Burgers equation. Suppose that the initial excitation $\mathbf{V}_p(\mathbf{x})$ represents an infinite sum of "inverse" modes $\mathbf{v}_r(\mathbf{x})$:

$$\mathbf{V}_p(\mathbf{x}) = \sum_{r=p}^{\infty} \mathbf{v}_r(\mathbf{x}). \tag{4.72}$$

In the two-dimensional case, the rth "inverse" mode may be constructed as a system of linear functions in equilateral triangles of a side L_r, densely covering the plane. Inside each triangle, in the rth mode, the velocity has the linear profile $\mathbf{v}_r(\mathbf{x}) = -\gamma_r(\mathbf{x}-\mathbf{x}_+)$, where $\mathbf{x}_+$ is the coordinate of the center of the triangle. It is easy to verify that the solution of the multi-dimensional Burgers equation for such an initial condition has the form

$$\mathbf{v}(\mathbf{x},t) = \frac{-\gamma(\mathbf{x}-\mathbf{x}_+)}{1-\gamma t} \tag{4.73}$$

and is valid inside a triangle of a size $L_r(t) = L_r(1-t\gamma_r)$. The quantity γ_r^{-1} has the dimension of time and, during the finite time $t_r = \gamma_r^{-1}$, the gradient of the field become infinite. In other words, at the moment of time $t = t_r$, the mode is transformed into a "straight" sawtooth wave with the universal behavior inside a new set of triangles and with the gradient $1/t$, which does not depend on the wavenumber and amplitude of the mode:

$$\mathbf{v}(\mathbf{x},t) = \frac{\mathbf{x}-\mathbf{x}_c}{t}, \tag{4.74}$$

where $\mathbf{x}_c$ now are the centers of triangles, which coincide with the vertices of the initial set of triangles. By considering the corresponding density of a gas of coalescing particles, we see that inside a "collapsing" triangle of a side length $L_r(t) = L_r(1-t\gamma_r)$, the density grows as

$$\rho(\mathbf{x},t) = \rho_0 \frac{1}{(1-t/t_p)^2}, \tag{4.75}$$

and the density ρ is equal to zero outside the "compensating" triangles. At the moment of time $t = t_r$, all light particles coalesce into heavy particles of a mass

$$m_r = \rho_0 L_r^2 \frac{\sqrt{3}}{4}, \tag{4.76}$$

and the coordinates of heavy particles coincide with the coordinates of the initial triangles $\mathbf{x}_+$.

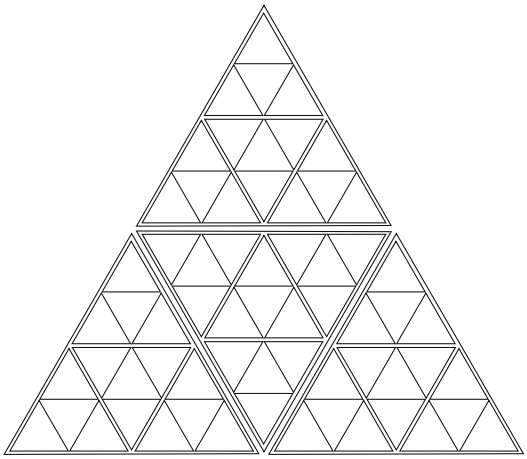

Fig. 4.16 Tessellation of the plane with hierarchical triangles, in which the modes of the multi-scale signal are defined.

For a multi-scale field, let us consider here a special case, when the ratio of the length scales of two consecutive modes is equal to $L_{r+1}/L_r = \varepsilon^{-1} = N = 2$. We also assume the presence of a special symmetry and special phase relations for all modes. In this case, a large triangle of the large-scale mode is divided into four small triangles of the consecutive small-scale mode so that no new shocks appear from the large-scale mode (see Fig. 4.16).

Let us now consider evolution of the vector field $\mathbf{V}_p(\mathbf{x})$ (4.72), which represents a superposition of an infinite number of "inverse" modes Suppose that evolution of the rth mode is characterized by the same nonlinear time t_r as in the one-dimensional case(4.47):

$$t_r = \gamma_r^{-1} = t_0/(2^{-(n+3)/2})^r. \tag{4.77}$$

Evolution of such a vector field is very similar to that considered by us in the one-dimensional case (4.59). So, for the gradient of the initial excitation $\mathbf{V}_p(\mathbf{x})$, we have the same expression (4.60) as in the one-dimensional case. The effective nonlinearity time of the small small-scale pth mode of the vector field (4.72) in the presence of all large-scale modes is, as before, determined by Eq. (4.61). Thus, after time $\tilde{t}_p$ has elapsed, there appear heavy particles of a mass m_p (4.76). The velocity of this particles is determined by the two-dimensional Weierstrass-Mandelbrot function $\mathbf{V}_{p+1}(\mathbf{x})$ (4.72), which is equal to the sum of all large-scale modes. At the moment of time $\tilde{t}_{p+1}$, we have a collision of four heavy particles for the next mode. Further process of the length-scale enlargement can be easily constructed by recursion. In Fig. 4.17, the hierarchical process of coalescence of particle is seen. While, in the one-dimensional case, the particle trajectories formed a structure similar to the flat model of an umbrella tree (see. [15]); in the two-dimensional case, this analogy is even more suitable. Whereas, as it has been shown, these structures possess the property of self-similarity.

In conclusion of this chapter, we note that despite the simplicity of the Burgers equation and availability of an exact solution, the evolution of fields in the frame-

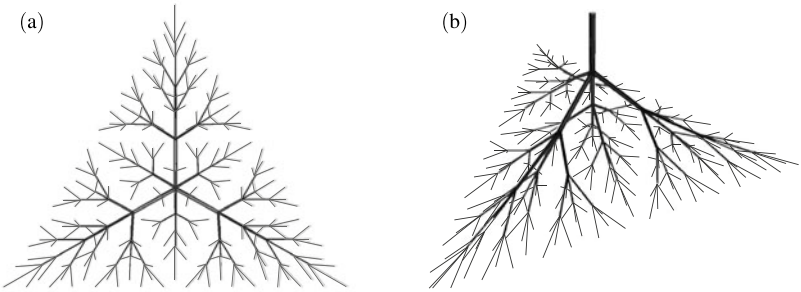

Fig. 4.17 Trajectories of particles for a multi-scale signal in the two-dimensional case, represented in the three-dimensional case (two coordinates vs time). The thickness of the trajectories reflects the mass of particles: **(a)** — top view; **(b)** — side view.

work of this equation is very diverse. Thereby the mechanical interpretation of solutions to the Burgers equation as evolution of a gas of coalescing particles is very intuitive and useful.

4.3 Problems to Chapter 4

Problem 1. Find the solution of the Burgers equation with the initial condition

$$v_0(x) = S[\delta(x) + \delta(x-\ell)] \quad (\ell > 0, \quad S > 0). \tag{4.78}$$

Plot $v(x,t)$ at $\mathrm{R} = S/2\mu \gg 1$ for different values of dimensionless time $\tau = 2St/\ell^2$.

Solution. In this case, the initial potential and the initial condition of the linear diffusion equation (3.78) are equal to:

$$s_0(x) = S[\Theta(x) + \Theta(x-\ell)],$$
$$\varphi_0(x) = 1 + \left(e^{-\mathrm{R}} - 1\right)\Theta(x) + \left(e^{-2\mathrm{R}} - e^{-\mathrm{R}}\right)\Theta(x-\ell).$$

By substituting the latter expression in (3.80), we have

$$\varphi(x,t) = 1 + \left(e^{-\mathrm{R}} - 1\right)\Phi\left(\frac{x}{2\sqrt{\mu t}}\right) + \left(e^{-2\mathrm{R}} - e^{-\mathrm{R}}\right)\Phi\left(\frac{x-\ell}{2\sqrt{\mu t}}\right).$$

Hence the solution of the Burgers equation is such:

$$v(x,t) = -\sqrt{\frac{\mu}{\pi t}}\,\frac{\left(e^{-\mathrm{R}} - 1\right)\exp\left(-\frac{x^2}{4\mu t}\right) + \left(e^{-2\mathrm{R}} - e^{-\mathrm{R}}\right)\exp\left(-\frac{(x-\ell)^2}{4\mu t}\right)}{1 + \left(e^{-\mathrm{R}} - 1\right)\Phi\left(\frac{x}{2\sqrt{\mu t}}\right) + \left(e^{-2\mathrm{R}} - e^{-\mathrm{R}}\right)\Phi\left(\frac{x-\ell}{2\sqrt{\mu t}}\right)}. \tag{4.79}$$

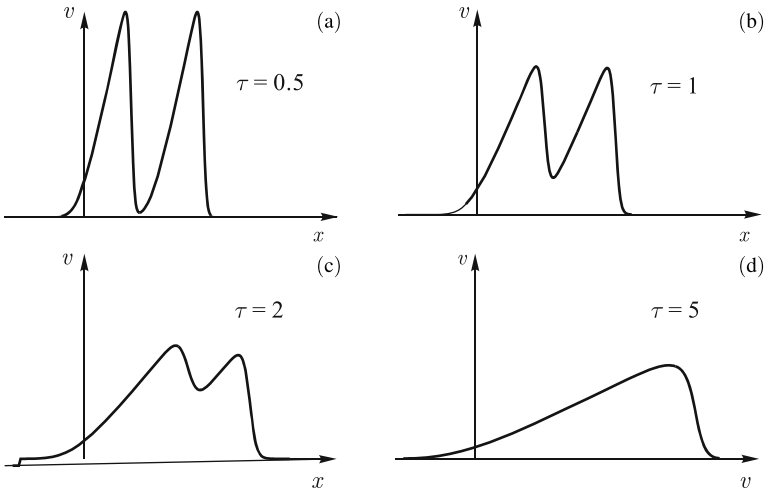

Fig. 4.18 Solution (4.79) of the Burgers equation at R = 16 illustrating the process of coalescence of triangular waves.

Its plots, constructed for different values of τ, are shown in Fig. 4.18. They illustrate the process of coalescence of two triangular waves corresponding to two delta functions in the initial condition (4.78).

Problem 2. Indicate the skeleton of the solution to the previous problem. By using the fact that the shock velocity is equal to the half-sum of the values of the field $v(x,t)$ before and after the shock, write down the equations of motion of the shocks and estimate the time of coalescence of the two triangular waves into one triangular wave.

Solution. In the beginning, the field's skeleton consists of separate triangles of the same area S bounded on the right by the shocks. Let us denote the shock coordinates $x_1(t)$ and $x_2(t)$. As long as the triangles do not overlap (see the top panel in Fig. 4.19), the shock coordinates can be easily found by using the fact that the areas of the triangles are conserved:

$$x_1(t) = \ell\sqrt{\tau}, \quad x_2(t) = \ell(1+\sqrt{\tau}), \quad \tau = \frac{t}{t^*} = \frac{2St}{\ell^2}. \tag{4.80}$$

At the moment of time

$$t^* = \frac{\ell^2}{2S} \quad (\tau = 1),$$

the left shock runs into the right one (the lower panel in Fig. 4.19), due to which the law of motion of the left shock changes. Let us find it by solving the equation of motion of the shock

$$\frac{dx_1(t)}{dt} = \frac{1}{t}\left(x_1(t) - \frac{\ell}{2}\right), \quad x_1(t^*) = \ell.$$

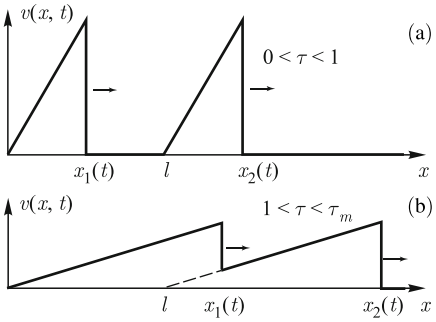

Fig. 4.19 Skeleton of the solution (4.79) of the Burgers equation.

As a result, we obtain

$$x_1(t) = \frac{\ell}{2}(\tau + 1). \tag{4.81}$$

By equating the coordinates of the right (4.80) and left (4.81) shocks, we find the sought-for time of their coalescence:

$$\tau_m = (1+\sqrt{2})^2 \approx 5.83.$$

Note. Initially (at $\tau < 1$), the field $v(x,t)$ consists of non-overlapping triangular waves, with the Reynolds number of each of them being equal to $\mathrm{R} = S/2\mu$. Further on, the merge into a single triangular wave with twice the area and Reynolds number. Thus the coalescence of the shocks leads *to the growth of the current Reynolds number.*

Problem 3. Find the shape of the smeared discontinuities of the averaged Lagrangian coordinate $\{y\}(x,t)$ (4.23) by taking into account two dominant terms in the vicinity of a shock.

Solution. Let, in the considered point of discontinuity of the function $\{y\}(x,t)$, two parabolas $\Pi_1(x)$ and $\Pi_2(x)$ intersect. By retaining the two corresponding terms in the sums (4.23), let us rewrite $\{y\}(x,t)$ in the following form:

$$\{y\}(x,t) \approx \frac{y_1 \exp\left(-\frac{1}{2\mu t}\left[s_1 t + \frac{(x-y_1)^2}{2}\right]\right) + y_2 \exp\left(-\frac{1}{2\mu t}\left[s_2 t + \frac{(x-y_2)^2}{2}\right]\right)}{\exp\left(-\frac{1}{2\mu t}\left[s_1 t + \frac{(x-y_1)^2}{2}\right]\right) + \exp\left(-\frac{1}{2\mu t}\left[s_2 t + \frac{(x-y_2)^2}{2}\right]\right)}. \tag{4.82}$$

Let us introduce new notation

$$x_1 = \frac{y_1 + y_2}{2}, \quad \ell = \frac{y_2 - y_1}{2}, \quad z = x - x_1.$$

By using this notation, after cancellation of common factors, we rewrite the expression (4.82) in the form

$$\{y\} \approx x_1 + \ell \frac{\exp\left(-\frac{s_2 t - z\ell}{2\mu t}\right) - \exp\left(-\frac{s_1 t + z\ell}{2\mu t}\right)}{\exp\left(-\frac{s_2 t - z\ell}{2\mu t}\right) + \exp\left(-\frac{s_1 t + z\ell}{2\mu t}\right)}.$$

From here, after simple manipulations, we finally have

$$\{y\} \approx \frac{y_1 + y_2}{2} + \frac{y_2 - y_1}{2} \tanh\left(\frac{\ell}{2\mu t}(x - x_1 - Ut)\right), \quad U = \frac{s_2 - s_1}{y_2 - y_1}.$$

Problem 4. By using the well-known formula

$$e^{\mathrm{R}\cos(\kappa x)} = I_0(R) + 2\sum_{n=1}^{\infty} I_n(\mathrm{R})\cos(n\kappa x),$$

where $I_n(z)$ is the modified Bessel function of the nth order, find the asymptotic behavior, at the linear stage, of the solution to the Burgers equation with the harmonic initial condition

$$v_0(x) = a\sin(\kappa x). \tag{4.83}$$

Investigate the dependence of the field amplitude at the linear stage on the initial amplitude a.

Solution. Let us first write down the corresponding solution of the linear diffusion equation (3.78):

$$\varphi(x,t) = I_0(R) + 2\sum_{n=1}^{\infty} I_n(\mathrm{R})\exp\left(-\frac{n^2\tau}{2\mathrm{R}}\right)\cos(nz). \tag{4.84}$$

Here we introduce the following notation:

$$z = \kappa x, \quad \tau = a\kappa t, \quad \mathrm{R} = \frac{a}{2\mu\kappa}.$$

By substituting (4.84) into (3.76) and retaining only the first terms in the numerator and denominator, we have:

$$v \approx \frac{2a}{\mathrm{R}} \frac{I_1(\mathrm{R})}{I_0(\mathrm{R})} e^{-\tau/2\mathrm{R}} \sin(z) \quad (\tau \gg \mathrm{R}). \tag{4.85}$$

In this case, it is appropriate to give the Reynolds number R a more suitable, from the viewpoint of acoustic applications, interpretation: it is equal to the ratio of the initial amplitude a of the field to the characteristic amplitude of development of nonlinear effects

$$a_n = \frac{1}{2\mu\kappa} \Rightarrow \mathrm{R} = \frac{a}{a_n}.$$

Apart from that, it is natural to investigate the dimensionless field

$$u = \frac{v}{a_n} = f(\mathrm{R})\,\exp\left(-\frac{\tau}{2\mathrm{R}}\right)\sin(z).$$

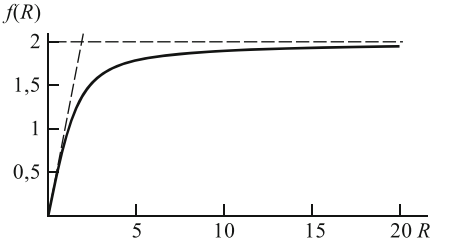

Fig. 4.20 Dimensionless amplitude of the initially harmonic field at the linear stage. As long as it practically coincides with the straight line R, nonlinear effects of evolution of the field $v(x,t)$ can be neglected.

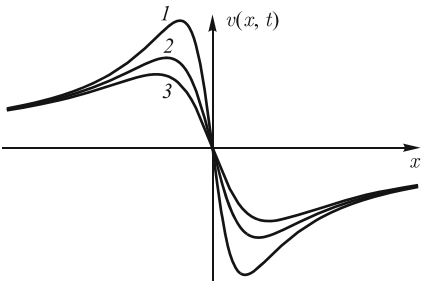

Fig. 4.21 Solution (4.85) of the Burgers equation at the moments of time $t_1, t_2 = 2t_1, t_3 = 3t_1$. "Anomalous" behavior of the solution is explained by the dominance of the diffusive smearing over the nonlinear inertial effects.

Here

$$f(\mathrm{R}) = 2\,\frac{I_1(\mathrm{R})}{I_0(\mathrm{R})},$$

where $f(\mathrm{R}) \simeq \mathrm{R}$, the field (4.85) replicates the solution of the linear equation with the initial condition (4.83), and it is possible to neglect the nonlinear effects. $f(\mathrm{R})$ is plotted in Fig. 4.20. It is seen that at large values of R, the function $f(\mathrm{R})$ saturates at the level of 2. This expresses a well-known fact that a nonlinear field with time "forgets" the initial condition and, in particular, its amplitude.

Problem 5. Find the solution of the Burgers equation, if

$$\varphi_0(x) = x^2.$$

Solution. The solution of the linear diffusion equation is here equal to

$$\varphi(x,t) = 2\mu t + x^2.$$

Accordingly, the solution of the Burgers equation has the following form:

$$v(x,t) = -\frac{x}{t}\,\frac{2}{1+z^2}, \quad z = \frac{x}{\sqrt{2\mu t}}. \tag{4.86}$$

It is plotted for three consecutive moments of time in Fig. 4.21. At first glance, the obtained solutions contradict intuition acquired by us: according to our understanding, at $x < 0$, where $v(x,t) > 0$, the field must move to the right, and the negative field, at $x > 0$, must move to the left. An analysis of the solution, and of the graphs, reveals that exactly the opposite happens. This is due to the fact that the effective

Reynolds number of the field (4.86) is close to unity, and the diffusive smearing dominates over the expected inertial effects.

References

1. O.V. Rudenko, S.N. Gurbatov, C.M. Hedberg, *Nonlinear Acoustics through Problems and Examples* (Trafford, 2010)
2. O.V. Rudenko, S.I. Soluyan, *Theoretical Foundations of Nonlinear Acoustics* (Plenum, New York, 1977)
3. S.N. Gurbatov, D.B. Crighton, The nonlinear decay of complex signals in dissipative media, Chaos **5**, 524–530 (1995)
4. J.R. Angilella, J.C. Vassilicos, Spectral, diffusive and convective properties of fractal and spiral fields, Physica D **124**, 23–57 (1998)
5. J.M. Burgers, *The Nonlinear Diffusion Equation* (D. Reidel, Dordrecht, 1974)
6. U. Frisch, *Turbulence: the Legacy of A.N. Kolmogorov* (Cambridge University Press, 1995)
7. S. Kida, Asymptotic properties of Burgers turbulence, J. Fluid Mech. **93**, 337–377 (1979)
8. S.A. Molchanov, D. Surgailis, W.A. Woyczynski, Hyperbolic asymptotics in Burgers' turbulence and extremal processes, Comm. Math. Phys. **168**, 209–226 (1995)
9. S.N. Gurbatov, A.N. Malakhov, A.I. Saichev, *Nonlinear Random Waves and Turbulence in Nondispersive Media: Waves, Rays and Particles.* (Manchester University Press, 1991)
10. S.N. Gurbatov, A.V. Troussov, The decay of multiscale signals — deterministic model of the Burgers turbulence, Phys. D **145**, 47–64 (2000)
11. E. Aurell, S.N. Gurbatov, I.I. Wertgeim, Self-preservation of large-scale structures in Burgers turbulence, Phys. Lett. A **182**, 109–113 (1993)
12. S.N. Gurbatov, G.V. Pasmanik, Self-preservation of large-scale structures in a nonlinear viscous medium described by the Burgers equation, J. Exp. Theoret. Phys. **88**, 309–319 (1999)
13. S.N. Gurbatov, A.I. Saichev, Degeneracy of one-dimensional acoustic turbulence at large Reynolds numbers, Sov. Phys. JETP **80**, 589–595 (1981)
14. M.V. Berry, Z.V. Lewis, On the Weierstrass–Mandelbrot fractal function, Proc. Roy. Soc. A **340**, 459–484 (1980)
15. B.B. Mandelbrot, *The Fractal Geometry of Nature* (Freeman, New York, 1982)
16. M. Vergassola, B. Dubrulle, U. Frisch, A. Noullez, Burgers' equation, devil's staircases and the mass distribution for large-scale structures, Astron. Astrophys. **289**, 325–356 (1994)